Chemistry–A European Journal

Supporting Information

Revisiting the Fundamental Nature of Metal-Ligand Bonding: An Impartial and Automated Fitting Procedure for Angular Overlap Model Parameters

Moritz Buchhorn, Robert J. Deeth, and Vera Krewald*

Angular Overlap Factors

Table 1: Angular overlap factors $F_{\sigma i}(\theta, \phi)$ as in [1].

i	$F_{\sigma i}(\theta, \phi)$
xy	$\frac{\sqrt{3}}{4}\sin(2\phi)(1-\cos(2\theta))$
yz	$\frac{\sqrt{3}}{2}\sin(\phi)\sin(2\theta)$
z^2	$\frac{1}{4}(1+3\cos(2\theta))$
xz	$\frac{\sqrt{3}}{2}\cos(\phi)\sin(2\theta)$
x^2-y^2	$\frac{\sqrt{3}}{4}\cos(2\phi)(1-\cos(2\theta))$

Table 2: Angular overlap factors $F_{\pi x i}(\theta, \phi, \psi)$ as in [1].

i	$F_{\pi x i}(\theta, \phi, \psi)$
xy	$\cos(2\phi)\sin(\theta)\sin(\psi)+\frac{1}{2}\sin(2\phi)\sin(2\theta)\cos(\psi)$
yz	$\cos(\phi)\cos(\theta)\sin(\psi)+\sin(\phi)\cos(2\theta)\cos(\psi)$
z^2	$-\frac{\sqrt{3}}{2}\sin(2\theta)\cos(\psi)$
xz	$-\sin(\phi)\cos(\theta)\sin(\psi)+\cos(\phi)\cos(2\theta)\cos(\psi)$
x^2-y^2	$-\sin(2\phi)\sin(\theta)\sin(\psi)+\frac{1}{2}\cos(2\phi)\sin(2\theta)\cos(\psi)$

Table 3: Angular overlap factors $F_{\pi y i}(\theta, \phi, \psi)$ as in [1].

i	$F_{\pi y i}(\theta, \phi, \psi)$
xy	$\cos(2\phi)\sin(\theta)\cos(\psi)-\frac{1}{2}\sin(2\phi)\sin(2\theta)\sin(\psi)$
yz	$\cos(\phi)\cos(\theta)\cos(\psi)-\sin(\phi)\cos(2\theta)\sin(\psi)$
z^2	$\frac{\sqrt{3}}{2}\sin(2\theta)\sin(\psi)$
xz	$-\sin(\phi)\cos(\theta)\cos(\psi)-\cos(\phi)\cos(2\theta)\sin(\psi)$
x^2-y^2	$-\sin(2\phi)\sin(\theta)\cos(\psi)-\frac{1}{2}\cos(2\phi)\sin(2\theta)\sin(\psi)$

Table 4: Simplified angular overlap factors $F_{\pi i}(\theta,\phi) = F_{\pi xi}(\theta,\phi,\psi=0) + F_{\pi yi}(\theta,\phi,\psi=0)$.

i	$F_{\pi i}(\theta,\phi)$
xy	$\cos(2\phi)\sin(\theta) + \frac{1}{2}\sin(2\phi)\sin(2\theta)$
yz	$\cos(\phi)\cos(\theta) + \sin(\phi)\cos(2\theta)$
z^2	$-\frac{\sqrt{3}}{2}\sin(2\theta)$
xz	$-\sin(\phi)\cos(\theta) + \cos(\phi)\cos(2\theta)$
x^2-y^2	$-\sin(2\phi)\sin(\theta) + \frac{1}{2}\cos(2\phi)\sin(2\theta)$

Discussion of Δ–values

A limited comparison with experimental data is possible for the values of Δ calculated from the AOM parameters. In the AOM, the d-orbital energy difference Δ in a tetrahedral complex is given as:

$$\Delta = \epsilon(t_{2g}) - \epsilon(e_g) = \frac{4}{3}e_\sigma - \frac{16}{9}e_\pi \tag{1}$$

Since orbitals and their energies are not observables, there is no direct connection with experiment. The approximation used most often is to resort to the first electronic transition: [1]

$$\Delta = E(^4T_2) - E(^4A_2) \tag{2}$$

In the special case of a tetrahedral d^7-system, the Tanabe-Sugano diagram for $B = 918\,\mathrm{cm}^{-1}$ and $C/B = 4.5$, the line of the $^4T_2(F)$ state is linear with a slope of 1.[2] In this case, the definitions of Δ are coincidentally equal. Table 5 shows calculated and experimental values for the ligand field splitting. While the ligand field splitting according to the AOM parametrization shows the correct trend, smaller splittings for heavier halides, the absolute values are consistently underestimated. The same observation can already be made in the ligand field splitting values calculated directly from the CASSCF and NEVPT2 states, although the NEVPT2 correction approaches the experimental value to within 200 cm^{-1}. An apparent mismatch arises from the fact that the CASSCF and NEVPT2 transition energies differ, although the fit of $\mathbf{V}_{LF}$ yields almost the same AOM parameters (see main text). The methods predict different Racah parameters (CASSCF: $B = 1200\,\mathrm{cm}^{-1}, C/B = 3.7$, NEVPT2: $B = 1000\,\mathrm{cm}^{-1}, C/B = 4.0$), so while the one-electron part of the ligand field Hamiltonian remains almost unaltered, the two-electron part changes significantly. Arguing with the Tanabe-Sugano diagrams this would mean different diagrams are necessary for both cases and Δ in Equation 2 is different to Δ in Equation 1. Consequently, the values cannot be compared directly. The trend in Δ, regardless of its definition, is reproduced by all of the calculations.

Table 5: Calculated and experimental values for Δ in cm^{-1}. Note that the theoretical and experimental definitions of Δ differ.

		$^4A_{2g} \Rightarrow {}^4T_{2g}/cm^{-1}$			
Complex	Δ_{AOM}/cm^{-1}	(CASSCF)	(NEVPT2)	$\Delta_{exp.}/cm^{-1}$	Source
$[CoCl_4]^{2-}$	2237	2100	3000	2825 - 3330	[3], [4], [5]
$[CoBr_4]^{2-}$	1999	1850	2700	2800	[4]
$[CoI_4]^{2-}$	1667	1500	2500	2700	[6]

Additional metal halides

For the extended series of metal halide complexes, we researched which coordination compounds exist and have been reported. The list in Table 6 makes no claim to be complete, but shows that most of the investigated complexes exist, either as solvated ion or as a subunit in a crystal lattice. Only Mn^{III} compounds were found.[7] We were unable to find (near-)tetrahedral Fe^{II} compounds for halides other than fluoride. All Cu^{II} fluorides we found are octahedrally coordinated,[8, 9] and for $[CuI_4]^{2-}$ we found no reported synthesis or analysis.

The AOM parameters for the series of metal halides resulting from our fitting procedure are shown in the main text. The results of bond length scans analogous to that shown for the cobalt complex are shown in Figure 1 to 5, with an overview of all data presented in Figure 6.

The AOM parameters and their ratios are similar for the same halides, as was pointed out in the main text. Here, we will discuss the deviations from the model system $[CoX_4]^{2-}$. For manganese, the optimized geometry is tetrahedral, as expected for a d^5 high-spin system. All other metal complexes show Jahn-Teller distortions that lead to different symmetries. $[FeX_4]^{2-}$ shows slightly bent bond angles, nevertheless the fit yields AOM parameters that are roughly identical.

$[NiX_4]^{2-}$ is distorted in an interesting way: there are two short, one intermediate and one long bond in the molecule. The difference between the bond lengths is about 0.02 Å. In every calculation, the AOM parameters of the short bonds are larger than the average at the respective length. Vice versa, the AOM parameters of the longer bonds are smaller than the average at the respective

Table 6: Experimental references for the metal halides $[MX_4]^{2-}$ where available.

X	Mn	Fe	Ni	Cu
F	none	[10]	[11, 12]	none
Cl	[13–16]	none	[13, 17]	[13, 18]
Br	[13, 15, 16, 19]	none	[13, 20]	[13, 21, 22]
I	[13, 15, 16]	none	[13]	none

Table 7: Angular overlap parameters E, e_σ, e_π and e_{ds} for homoleptic copper halides $[CuX_4]^{2-}$. To avoid overparameterization, a grouped fit was performed where the additional restraint $e_{\lambda,L} = e_{\lambda,L'}$ is imposed.

X	E/cm^{-1}	$e_\sigma/\mathrm{cm}^{-1}$	e_π/cm^{-1}	e_{ds}/cm^{-1}
F	−1 822 578(32)	5012(26)	2107(29)	402(31)
Cl	−1 835 247(26)	2949(37)	1069(29)	141(24)
Br	−1 841 118(51)	2457(35)	845(27)	85(32)
I	−1 847 925(25)	1919(34)	612(26)	20(27)

length. This illustrates the mutual influence of ligands on each other, and that not only their chemical nature, but also their relative bond length is important.

The copper complexes have D_{2d} symmetry, which would require the consideration of d-s mixing[23] or the introduction of coordination voids.[24] The least-squares fit is able to find a set of E, e_σ and e_π parameters which represent the d-orbital energies with the smallest deviation to the original V_{LF}. However, the overall fitting costs are very high and the d-orbital energies are reproduced less well than in the other examples. Inclusion of d-s mixing significantly improves the fit and lowers the cost. Preliminary results with an additional d-s mixing parameter e_{ds} for the copper halides are shown in Table 7. The equations used for the fit are derived and presented in [25].

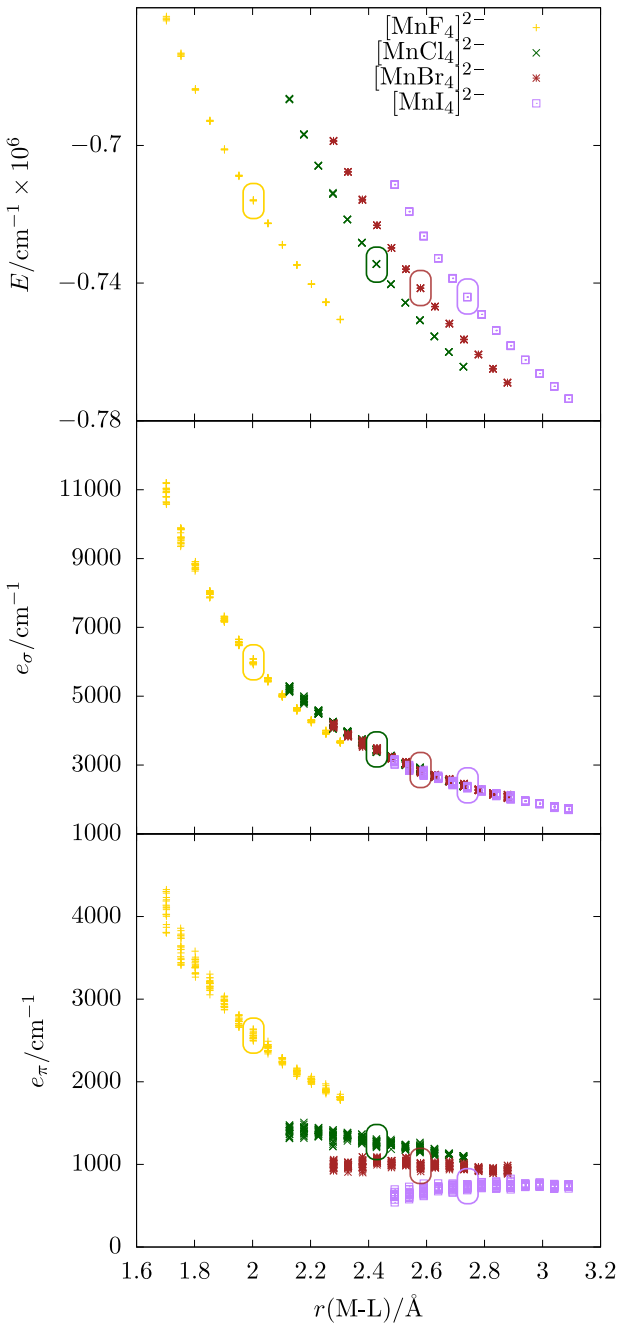

Figure 1: E, e_σ and e_π of homoleptic manganese halides for different bond lengths. The respective equilibrium bond lengths are highlighted with boxes around the data points.

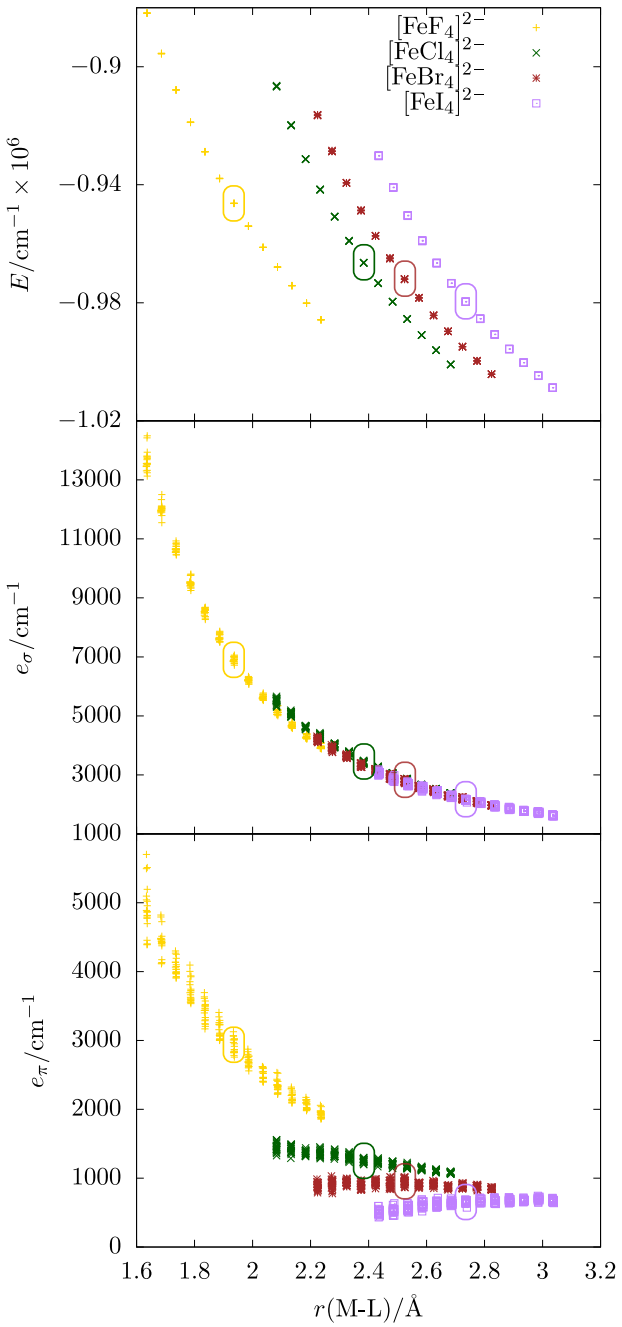

Figure 2: E, e_σ and e_π of homoleptic iron halides for different bond lengths. The respective equilibrium bond lengths are highlighted with boxes around the data points.

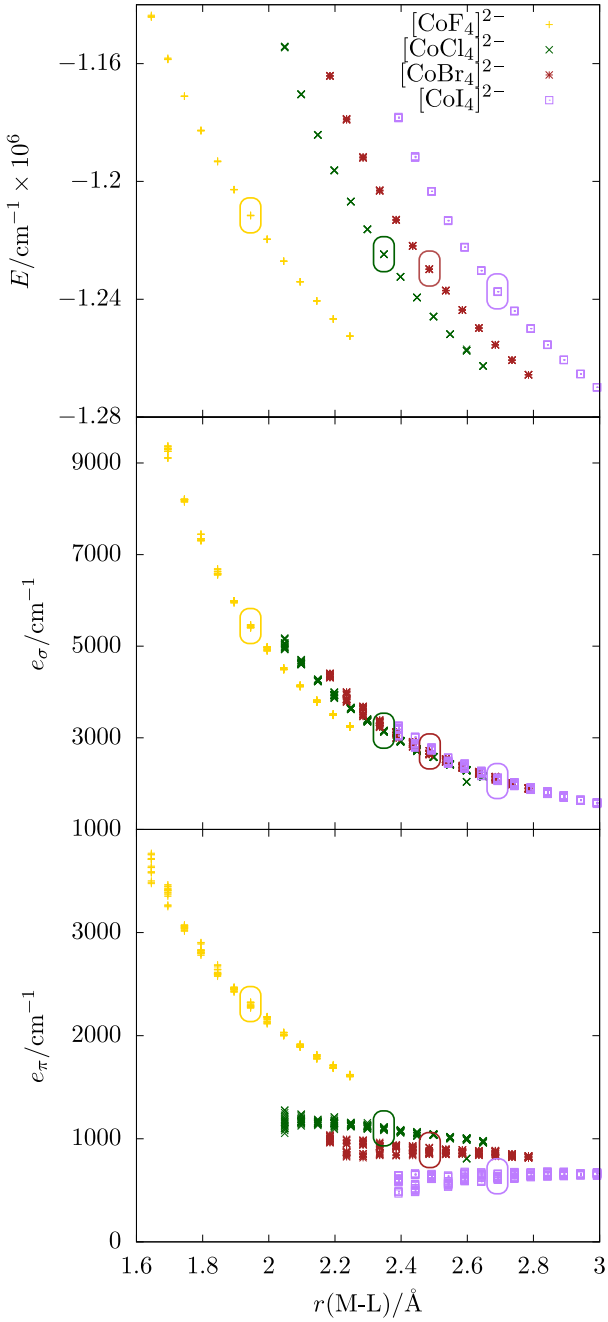

Figure 3: E, e_σ and e_π of homoleptic cobalt halides for different bond lengths. The respective equilibrium bond lengths are highlighted with boxes around the data points.

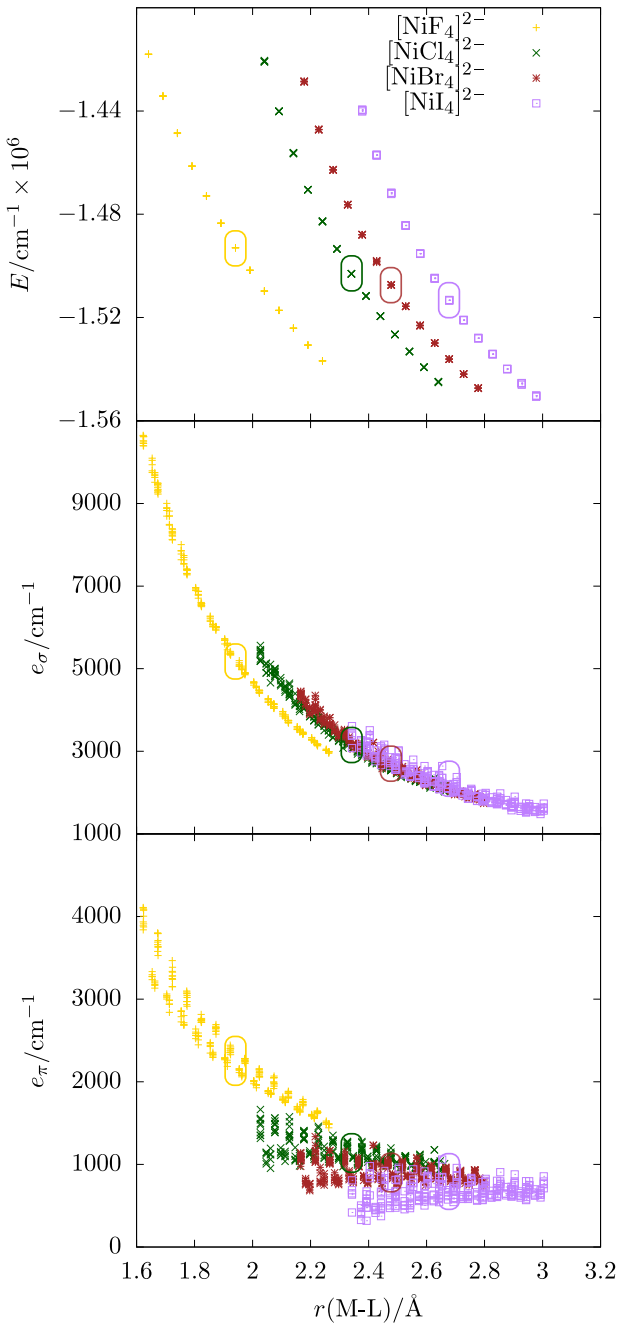

Figure 4: E, e_σ and e_π of homoleptic nickel halides for different bond lengths. The respective equilibrium bond lengths are highlighted with boxes around the data points.

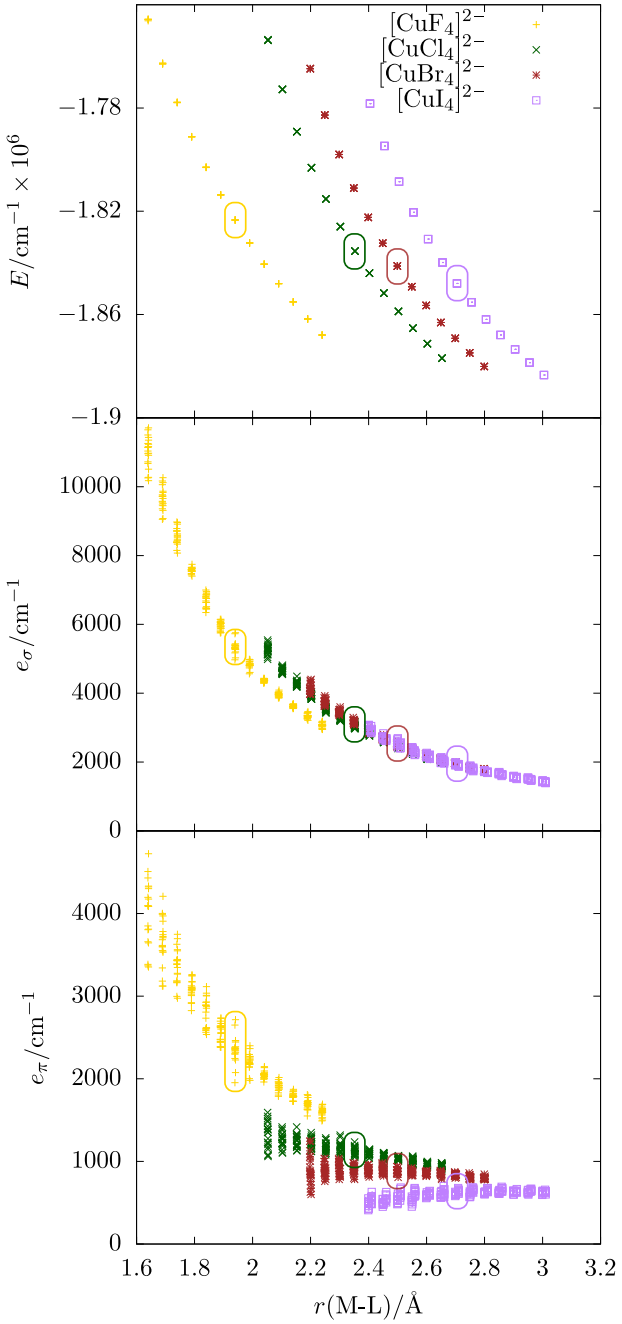

Figure 5: E, e_σ and e_π of homoleptic copper halides for different bond lengths. The respective equilibrium bond lengths are highlighted with boxes around the data points.

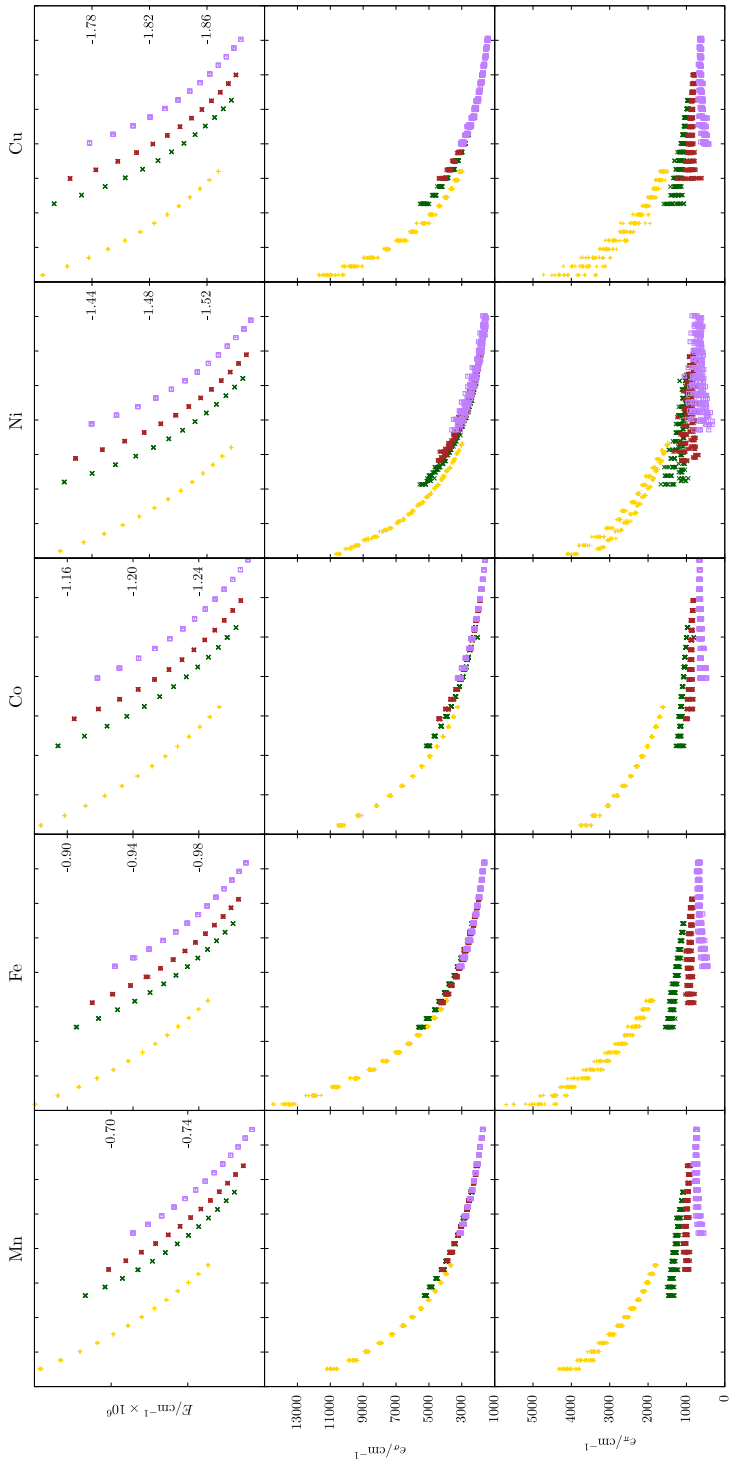

Figure 6: E, e_σ and e_π of homoleptic metal halides for different bond lengths as an overview of the preceding plots.

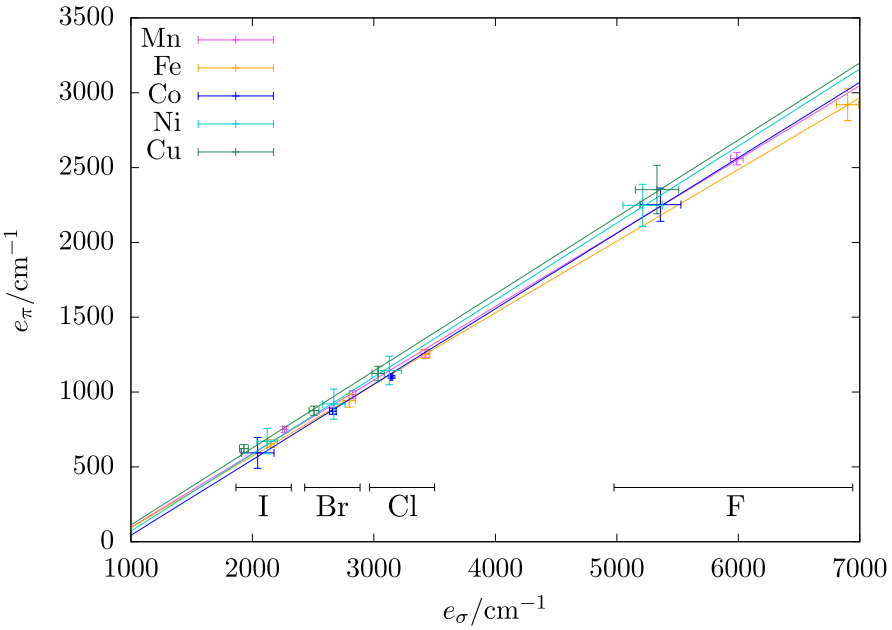

Figure 7: 2D-spectrochemical series for different metal halides, each metal with a different color. Error bars indicate the standard deviation. Regression line functions are:
Mn: $e_\pi = 0.4915 e_\sigma - 394\mathrm{cm}^{-1}$
Fe: $e_\pi = 0.4786 e_\sigma - 385\mathrm{cm}^{-1}$
Co: $e_\pi = 0.5043 e_\sigma - 461\mathrm{cm}^{-1}$
Ni: $e_\pi = 0.5145 e_\sigma - 443\mathrm{cm}^{-1}$
Cu: $e_\pi = 0.5144 e_\sigma - 403\mathrm{cm}^{-1}$

Discussion of technical details

Differences between CASSCF and NEVPT2

As the underlying wavefunction method, CASSCF or CASSCF/NEVPT2 can be chosen. Our results show that this choice does not alter the e_λ parameters significantly. It was observed already that CASSCF results are fitted more easily than NEVPT2 results.[26] We can confirm that observation, since the standard deviation is strictly smaller when fitting CASSCF results with the AOM compared to the NEVPT2 fit. There appears to be a problem with the NEVPT2 correction: according to Jung *et al.*, the energies of the states are changed in the order of energy, not in the order of states.[27] If the energetic ordering of the states were changed by the NEVPT2 correction, the aiLFT matrix elements would not be replaced accordingly. We found this to be a problem in some mixed halide calculations, leading to odd AOM parameter sets. For this reason, all shown results are fits of the CASSCF matrix without the NEVPT2 correction.

Choice of basis set

With CASSCF or CASSCF/NEVPT2 as the underlying wavefunction method, a basis set dependence is expected for the absolute energies. Table 8 shows the fitting results for $[CoCl_4]^{2-}$ with the Karlsruhe def2-SVP, def2-TZVP and def2-QZVP basis sets. E decreases with increasing basis set size, the other AOM parameters do not show a trend.

Influence of implicit solvation models

To assess the influence of environmental corrections on the AOM parameters, three different fits based on CASSCF calculations in vacuum and with the CPCM and SMD solvation models for water were made, see Figure 8. E is strongly affected, which is in good agreement with the concept of E being a spherical contribution assuming that the solvation shell is highly symmetric in the given geometry. In contrast, the AOM parameters show a very limited dependence on the solvation model.

The fact that the non-spherical contribution of the ligands is nearly independent of this (neglecting some outliers with the cpcm model) is also fitting. All calculations in the main text are performed without any solvation model,

Table 8: AOM parameters and E of $[CoCl_4]^{2-}$ for different basis sets.

basis set	E/cm^{-1}	E_{rel}/cm^{-1}	$e_\sigma/\mathrm{cm}^{-1}$	e_π/cm^{-1}
def2-SVP	-1221831	4049	3235(15)	1183(14)
def2-TZVP	-1224735	1145	3146(10)	1101(9)
def2-QZVP	-1225880	0	3164(17)	1106(13)

but we note explicitly that a solvent model can be included without any loss in accuracy or notable increase in computational cost.

Origin of deviations in the fitted AOM parameters

At each bond length, five structures are generated by changing their bond angle, fulfilling the requirements stated in the main text. A separate set of parameters is assigned to each bond, so four AOM parameter sets are obtained per tetrahedral complex. For a homoleptic complex, 20 parameter sets are obtained. With the heteroleptic complexes, this number decreases, since the parameter sets then belong to different M-L bonds.

As already pointed out, an ideal tetrahedral system is underdetermined in terms of an AOM parameterization. The procedure employed here can solve this problem to some extent, but especially for the heteroleptic complexes, large deviations are found. Within a single calculation, parameters associated with the same ligand are always very close to each other, but in a set (same bond lengths, slightly different bond angles), the differences between the obtained parameters can be large. Most often, there is one strong outlier, while the other four calculations yield similar parameter sets. These outliers can be easily identified by looking at the data. In the plots in the main text, some of these outliers were removed. In the plots in the SI, all obtained data points are shown.

It is not entirely clear what the cause of the observed scattering of AOM parameters is, but some observations were made that indicate the origin of this problem to be rooted in the electronic structure of these complexes rather than the fitting procedure itself. The structures are extremely similar, no distinctive features can be found for structures with stark outliers. The d orbital energies (which are the eigenvalues of $\mathbf{V}_{LF}$) are unremarkable. The equation systems resulting from the structures do not show unexpected values, the least squares fit converges without errors and reliably finds the only minimum. Numerical precision does not seem to be an issue, since $\mathbf{V}_{LF}$ rounded to fewer digits yields roughly the same AOM parameters.

We noted that the scattering becomes stronger at shorter bond lengths, where the molecule is in a chemically unrealistic situation. At short bond lengths, there is most often not only one strong outlier, but all the sets significantly differ from each other. We observed that the d orbitals at shorter bond lengths are not pure anymore, so it could be possible that aiLFT and the AOM cannot properly describe these molecules anymore. While the data sets presented in this contribution are obtained with equal bond length variations about the equilibrium distance, it is obviously equally possible to perform a bond length scan that contains more data points at longer bond lengths; this procedure would be expected to produce fewer outliers.

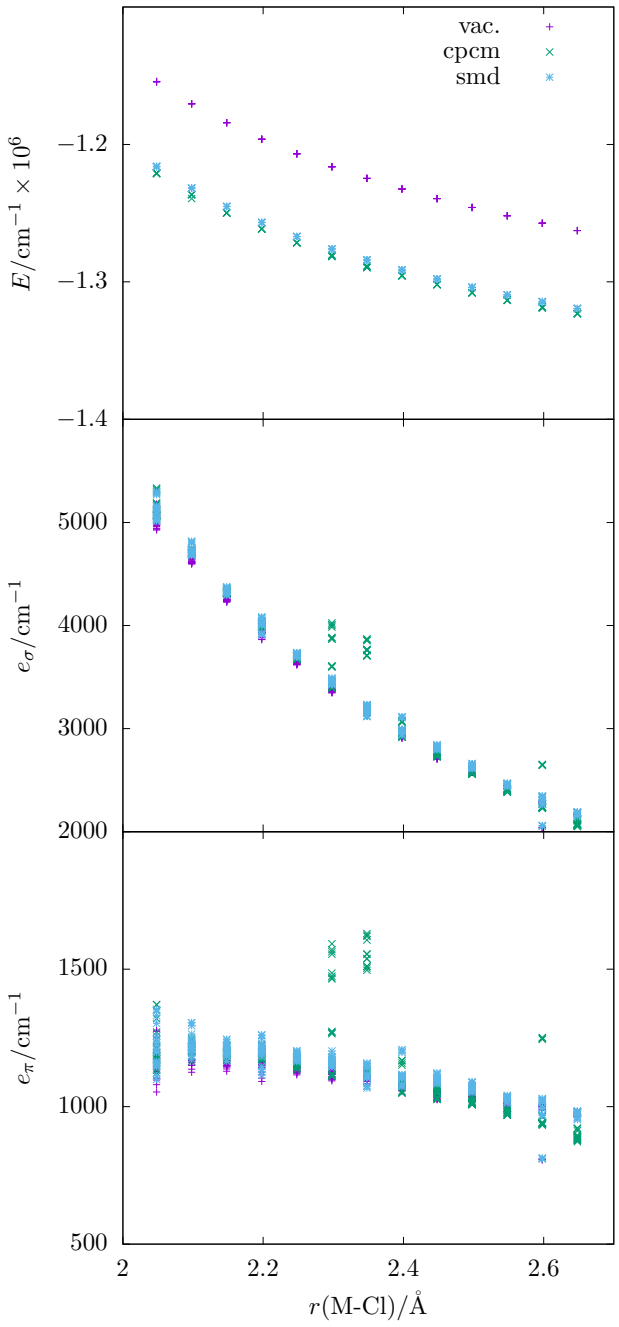

Figure 8: AOM parameters for $[CoCl_4]^{2-}$ with and without implicit solvation.

AOM parameters of mixed complexes

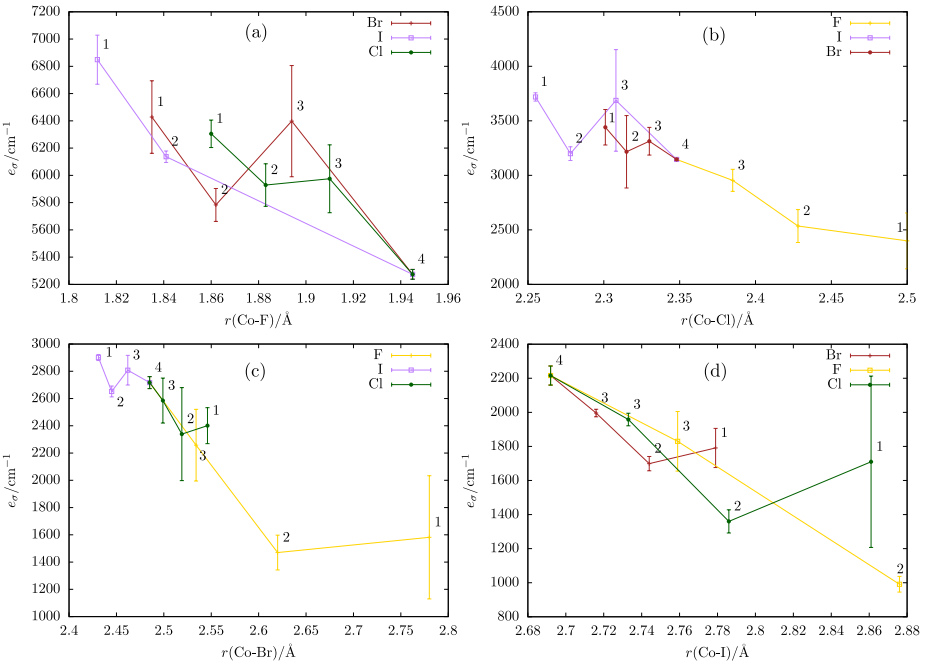

Figure 9: e_σ parameters with of Co−X for different, fully relaxed $[\mathrm{CoX}_n\mathrm{Y}_{4-n}]^{2-}$ complexes. The data shown are averaged over five data points each, and the error bars indicate the resulting standard deviation. The number at each data point indicates the X atom count, and the legend shows which other halide is present in the complex.

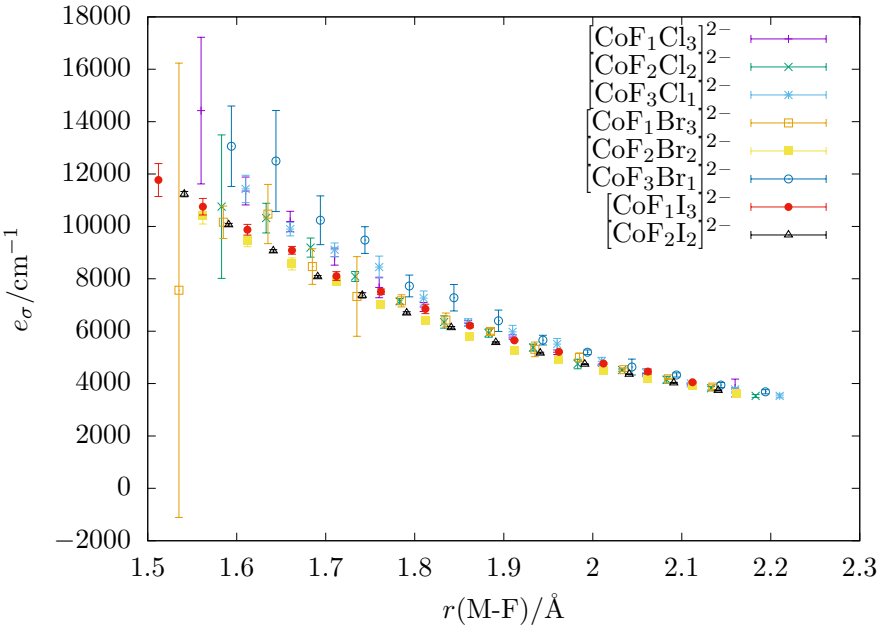

Figure 10: e_σ of the M-F bond length in various heteroleptic complexes.

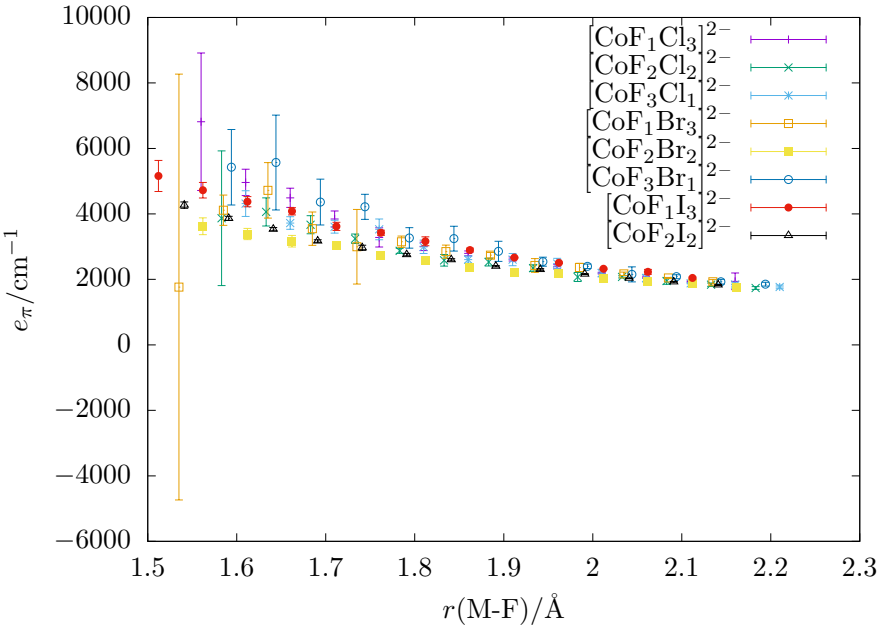

Figure 11: e_π of the M-F bond length in various heteroleptic complexes.

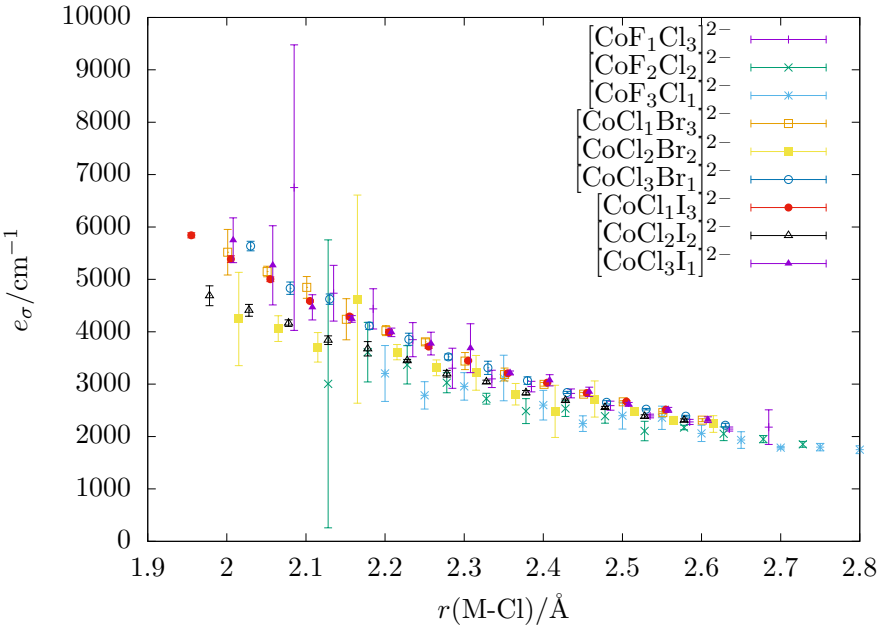

Figure 12: e_σ of the M-Cl bond length in various heteroleptic complexes.

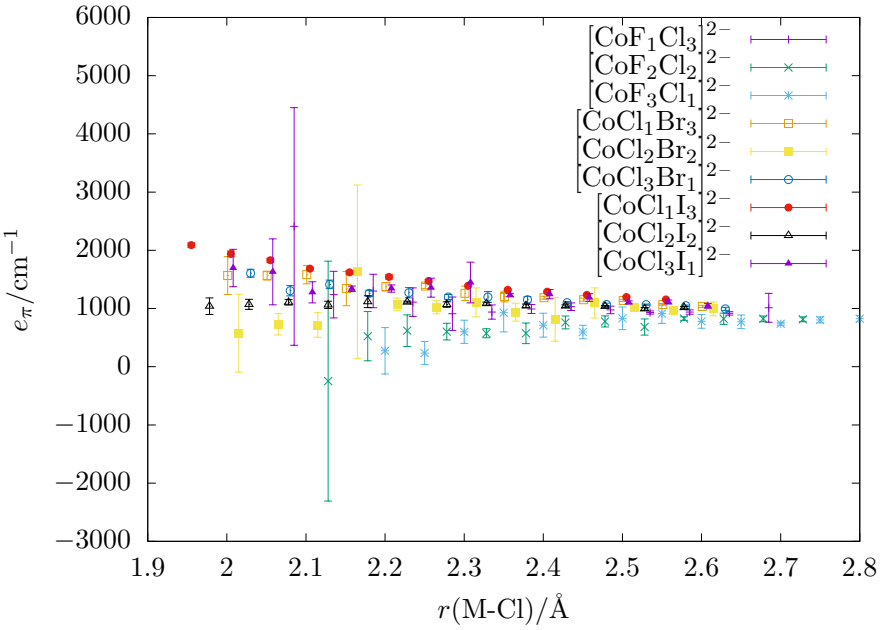

Figure 13: e_π of the M-Cl bond length in various heteroleptic complexes.

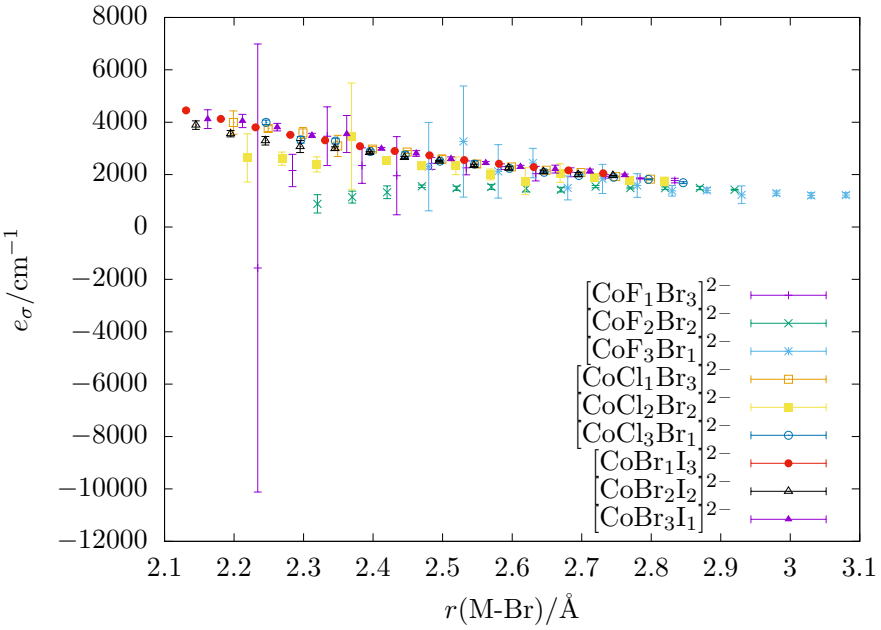

Figure 14: e_σ of the M-Br bond length in various heteroleptic complexes.

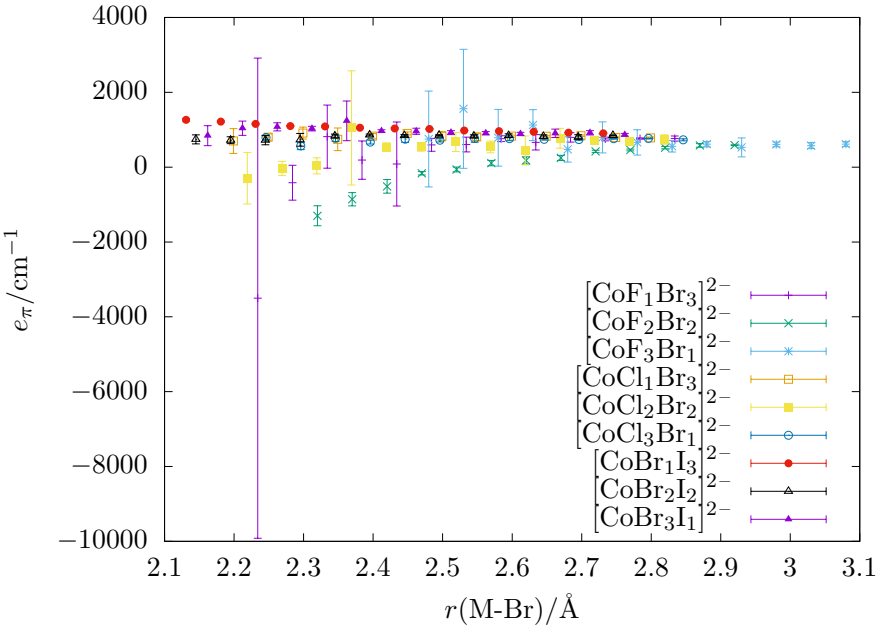

Figure 15: e_π of the M-Br bond length in various heteroleptic complexes.

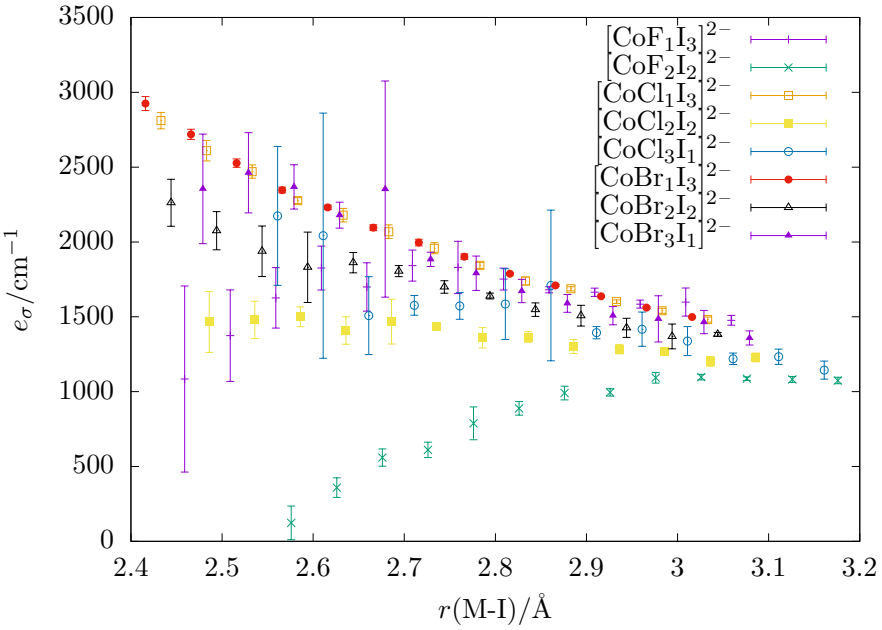

Figure 16: e_σ of the M-I bond length in various heteroleptic complexes.

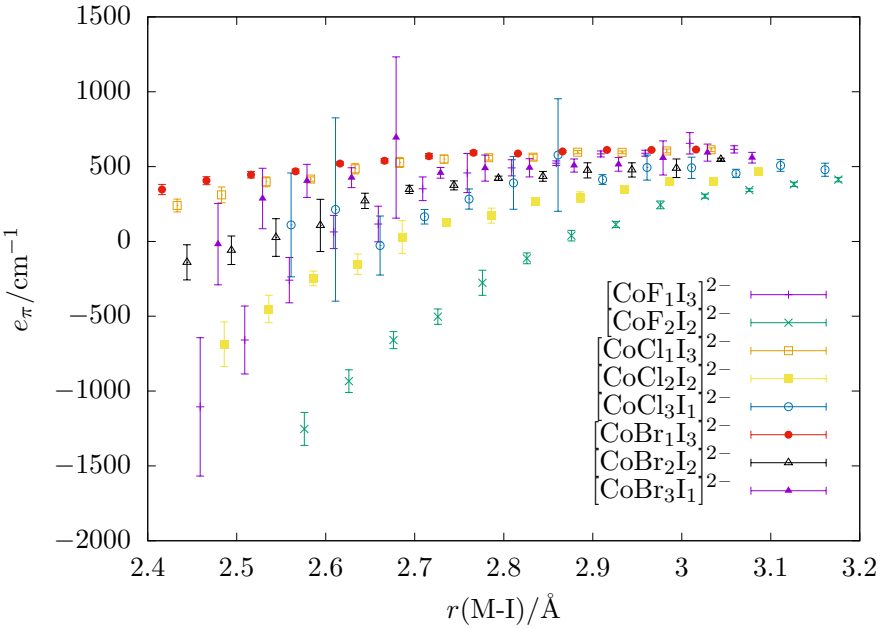

Figure 17: e_π of the M-I bond length in various heteroleptic complexes.

References

[1] B. N. Figgis, M. A. Hitchman, *Ligand Field Theory and Its Applications*, 1st ed., Wiley-VCH, New York, **2000**.

[2] Y. Tanabe, S. Sugano, *J. Phys. Soc. Japan* **1954**, *9*, 766–779.

[3] S. Buffagni, T. M. Dunn, *Nature* **1960**, *188*, 937–938.

[4] K. Kojima, J. Matsuda, *Bull. Chem. Soc. Jpn.* **1986**, *59*, 859–863.

[5] W. D. Horrocks, D. A. Burlone, *J. Am. Chem. Soc.* **1976**, *98*, 6512–6516.

[6] L. H. Gade, *Koordinationschemie*, Wiley-VCH, **1998**.

[7] M. Molinier, W. Massa, *Z. Naturforsch. B* **1992**, *47*, 783–788.

[8] K. Knox, *J. Chem. Phys.* **1959**, *30*, 991–993.

[9] D. Babel, M. Otto, *Z. Naturforsch. B* **1989**, *44*, 715–720.

[10] J. W. Lauher, J. A. Ibers, *Inorg. Chem.* **1975**, *14*, 348–352.

[11] W. Rüdorff, J. Kändler, D. Babel, *Z. Anorg. Allg. Chem.* **1962**, *317*, 261–287.

[12] M. K. Chaudhuri, S. K. Ghosh, Z. Hiese, *J. Chem. Soc. Dalton Trans.* **1984**, 1763.

[13] N. S. Gill, R. S. Nyholm, *J. Chem. Soc.* **1959**, 3997.

[14] F.-D. Tsay, L. Helmholz, *J. Chem. Phys.* **1969**, *50*, 2642–2650.

[15] V. Morad, I. Cherniukh, L. Pöttschacher, Y. Shynkarenko, S. Yakunin, M. V. Kovalenko, *Chem. Mater.* **2019**, *31*, 10161–10169.

[16] B. R. Sundheim, E. Levy, B. Howard, *J. Chem. Phys.* **1972**, *57*, 4492–4496.

[17] M. B. Meredith, C. H. McMillen, J. T. Goodman, T. P. Hanusa, *Polyhedron* **2009**, *28*, 2355–2358.

[18] L. Helmholz, R. F. Kruh, *J. Am. Chem. Soc.* **1952**, *74*, 1176–1181.

[19] K. Hasebe, T. Asahi, K. Gesi, *Acta Cryst. C* **1990**, *46*, 759–762.

[20] D. A. Fine, *Inorg. Chem.* **1965**, *4*, 345–350.

[21] B. Morosin, E. C. Lingafelter, *Acta Cryst.* **1960**, *13*, 807–809.

[22] P. S. Braterman, *Inorg. Chem.* **1963**, *2*, 448–452.

[23] D. W. Smith, *Inorg. Chim. Acta* **1977**, *22*, 107–110.

[24] R. J. Deeth, M. Gerloch, *Inorg. Chem.* **1984**, *23*, 3846–3853.

[25] R. J. Deeth, D. L. Foulis, *Phys. Chem. Chem. Phys.* **2002**, *4*, 4292–4297.

[26] S. K. Singh, J. Eng, M. Atanasov, F. Neese, *Coord. Chem. Rev.* **2017**, *344*, 2–25.

[27] J. Jung, M. Atanasov, F. Neese, *Inorg. Chem.* **2017**, *56*, 8802–8816.